University of Nebraska - Lincoln
DigitalCommons@University of Nebraska - Lincoln

Civil and Environmental Engineering Faculty Publications

Civil and Environmental Engineering

2014

Geological CO2 storage: Incorporation of pore-pressure/stress coupling and thermal effects to determine maximum sustainable pressure limit

Seunghee Kim

Seyyed Abolfazl Hosseini

Follow this and additional works at: https://digitalcommons.unl.edu/civilengfacpub

This Article is brought to you for free and open access by the Civil and Environmental Engineering at DigitalCommons@University of Nebraska - Lincoln. It has been accepted for inclusion in Civil and Environmental Engineering Faculty Publications by an authorized administrator of DigitalCommons@University of Nebraska - Lincoln.

Available online at www.sciencedirect.com

ScienceDirect

Energy Procedia 63 (2014) 3339 – 3346

Energy Procedia

GHGT-12

Geological CO_2 storage: Incorporation of pore-pressure/stress coupling and thermal effects to determine maximum sustainable pressure limit

Seunghee Kim[a,*], Seyyed Abolfazl Hosseini[b]

[a]*Western New England University, 1215 Wilbraham Rd, Springfield, MA 01119, USA*
[b]*Bureau of Economic Geology, The University of Texas at Austin, 10100 Burnet Rd, Austin, TX 78758, USA*

Abstract

Ensuring geomechanical integrity is a critical factor in the successful operation of geological CO_2 storage. Injecting pressurized cold CO_2 into a reservoir will trigger two geomechanically coupled phenomena, hydro- and thermomechanical coupling, which should be taken into account when determining the maximum sustainable pressure limit. In this regard, we briefly introduce poroelastic and thermally induced stresses as cold fluid is injected into a geologic formation. We then propose new equations that incorporate pore-pressure/stress coupling and thermal stress effects to calculate for various stress regimes—including normal-, reverse-, and strike-slip faulting—the maximum pressure limit before reactivation of preexisting fractures. The suggested equations are tested for a case study in the literature in which the maximum pressure limit was estimated based on complex numerical simulations. Lastly, sensitivity analysis based on these suggested equations sheds light on how sensitive the maximum pressure limit is to several input parameters, including saturated rock density, Biot's coefficient, Poisson's ratio, initial total horizontal-to-vertical stress ratio, temperature drop, and Young's modulus.

© 2014 The Authors. Published by Elsevier Ltd. This is an open access article under the CC BY-NC-ND license (http://creativecommons.org/licenses/by-nc-nd/3.0/).
Peer-review under responsibility of the Organizing Committee of GHGT-12

Keywords: Geological CO_2 storage; Shear reactivation; Maximum sustainable pressure limit; Pore-pressure/stress coupling; Thermal stress effect

* Corresponding author. Tel.: +1-413-782-1653; fax: +1-413-796-2116.
E-mail address: seunghee.kim@wne.edu

1876-6102 © 2014 The Authors. Published by Elsevier Ltd. This is an open access article under the CC BY-NC-ND license (http://creativecommons.org/licenses/by-nc-nd/3.0/).
Peer-review under responsibility of the Organizing Committee of GHGT-12
doi:10.1016/j.egypro.2014.11.362

1. Introduction

Ensuring geomechanical integrity is a critical factor in the successful operation of geological CO_2 storage [1]. Injection of pressurized cold CO_2 into a geologic formation will trigger two geomechanically coupled phenomena: (1) hydromechanical coupling, and (2) thermomechanical coupling [2, 3]. Therefore, in an attempt to avoid undesirable geomechanical failures, these two coupled phenomena should be taken into account when estimating the maximum sustainable pressure limit [4]. In this manuscript, we briefly introduce poroelastically and thermally induced stresses as cold CO_2 is injected with higher pressure into a reservoir. We then propose new equations that incorporate pore-pressure/stress coupling and thermal stress effects with which maximum pressure limit can be analytically calculated for different stress regimes such as normal-, reverse-, and strike-slip faulting. Lastly, for verification purposes, we test the proposed equations for a case study in the literature and explore the sensitivity of the maximum pressure limit to several input parameters.

2. Poroelastic and Thermal Stresses

When a fluid, whether similar to an original formation fluid or different from it, is injected into a geologic formation, it causes pore-pressure buildup and poroelastic effects [5-7]. If the injected fluid retains a different temperature, thermal stress effect would be added to it [8, 9]. We introduce the poroelastic and thermal stress effects in this section.

2.1. Poroelastic Stress

Many production fields have reported that stress decreases in response to a drop in pore pressure during fluid extraction [10-14]. For example, the ratio of change in total horizontal stress to change in pore pressure was reported to range $0.34 \leq \Delta\sigma_h/\Delta p < 1.18$ in many petroleum production sites [5]. Likewise, fluid injection will cause pore pressure to rise and total stress to increase, as well. Recent studies suggest that both total vertical and horizontal stresses change when coupled with a change in pore pressure [5, 6, 15]. For example, let us consider an ideal case where a fluid is injected with a constant injection rate at a point into a saturated linear-elastic porous medium. The ratio of change in total stress to change in pore pressure $\Delta\sigma/\Delta p$ can be expressed as a function of Biot's coefficient α, Poisson's ratio v, and the Boltzmann variable $\xi=((x_k x_k)/c_d/t)^{1/2}$ where c_d denotes hydraulic diffusivity and t denotes time elapsed after the injection [5, 16]:

$$\frac{\Delta\sigma_{ij}(x,t)}{\Delta p(x,t)} = \frac{\alpha(1-2v)\{\delta_{ij}[erfc((1/2)\xi)-(2/\xi^2)g(\xi)]+(x_i x_j/r^2)[erfc((1/2)\xi)+(6/\xi^2)g(\xi)]\}}{2(1-v)erfc((1/2)\xi)}$$

$$\text{where, } g(\xi)=\frac{1}{2\sqrt{\pi}}\int_0^{\xi} s^2\exp\left(-\frac{1}{4}s^2\right)ds = erf\left(\frac{1}{2}\xi\right)-\frac{\xi}{\sqrt{\pi}}\exp\left(-\frac{1}{4}\xi^2\right) \tag{1}$$

If stresses evolve corresponding to pore-pressure buildup, Mohr's circle is going to expand or shrink as well as shift toward a failure envelope as fluid injection is imposed at a reservoir, depending on an initial stress regime [17, 18]. Therefore, the pore-pressure/stress coupling effect needs to be taken into account when estimating the maximum sustainable pressure limit. We define the pore-pressure/stress coupling ratios, β_h and β_v, to represent changes in total horizontal and vertical stresses to change in pore pressure for general cases as follows:

$$\beta_h = \frac{\Delta\sigma_h}{\Delta p} = \frac{\Delta\sigma_H}{\Delta p} \text{ and } \beta_v = \frac{\Delta\sigma_v}{\Delta p} \tag{2}$$

These values converge to $\beta_h=\alpha(1-2\nu)/(1-\nu)$ and $\beta_v=(\alpha/2)(1-2\nu)/(1-\nu)$, respectively, for a homogeneous infinite medium [5]. A summary of static analytical solutions for other reservoir shapes are provided in Safari et al. [15].

2.2. Thermal Stress

Injected CO_2 is likely to be colder than original formation fluid [19]. For example, the bottom-hole temperature of injected CO_2 is ~44°C colder than the formation brine at the Cranfield pilot test site [20]. Fluid injection rate affects the bottom-hole temperature at the injection well as it affects the heat exchange between CO_2 and ambient rock before arriving at the bottom hole [21]. That is, the slower the injection rate, the more heat the fluid gains from the ambient geothermal. Regardless of how much colder it would be, injecting colder fluid will cause thermal contraction and subsequent decreases in stresses, which is an opposite effect of what volume expansion and increases in stresses driven by fluid injection do. If temperature drops by ΔT, total vertical and horizontal stresses decrease as follows (assuming a fully constrained sediment [4]):

$$\Delta\sigma^T = \frac{\alpha_T E \Delta T}{1-2\nu} \tag{3}$$

where α_T indicates the coefficient of thermal expansion and E represents Young's modulus. The thermal stress drop could be significant or not depending on the temperature drop and relevant material property. For example, if temperature were to drop by ΔT=15°C in a reservoir whose property is given as $\alpha_T=1\times10^{-5}$/K, E=17.6GPa and ν=0.15, total stresses would decrease by $\Delta\sigma^T$~3.8MPa via shrinkage [20]. The areal effect of thermal diffusion is narrower than the areal effect of poroelastic stress disturbance because it has to cool down ambient rock when the injected CO_2 is cold [3].

3. Maximum Sustainable Pressure Limit

It is often necessary to quickly calculate the maximum sustainable pressure limit to reduce the uncertainty of geomechanical instability. In this section we propose a failure criterion and equations that incorporate poroelastic and thermal stress effects with which the maximum pressure limit for different stress regimes can be quickly estimated.

3.1. Failure Criterion

Reactivation of preexisting fractures via shear slip (i.e., induced seismicity) is likely to occur, in most cases, prior to shear failures of intact rock or tensile fractures [17, 22], so it will determine the maximum sustainable pressure limit p_{max}. In 2D analysis, the magnitude of shear stress τ and normal stress σ_n acting on a preexisting fracture plane that has angle θ with respect to minor principal stress σ_3 can be expressed as:

$$\tau = \frac{\sigma_1-\sigma_3}{2}\sin 2\theta \text{ and } \sigma_n = \frac{\sigma_1+\sigma_3}{2} + \frac{\sigma_1-\sigma_3}{2}\cos 2\theta \tag{4}$$

where σ_1 represents major principal stress.

The Mohr-Coulomb shear failure criterion then can be used to evaluate the slip of the fault plane:

$$\tau = c + (\sigma_n - \alpha p_{\max})\mu \tag{5}$$

where τ is the critical shear stress for the shear slip to occur, c is the cohesion of the preexisting fault plane, and μ (=tanφ where φ denotes the fault friction angle) is the coefficient of the fault friction [23]. Assuming zero cohesion

c=0 for the preexisting fractures and inserting Equation 4 into Equation 5, the maximum pressure limit p_{max} on the verge of reactivating faults can be expressed as follows [23]:

$$p_{\max} = \frac{1}{\alpha}\left[\frac{1}{2}(\sigma_1+\sigma_3)+\frac{1}{2}(\sigma_1-\sigma_3)\cos 2\theta - \frac{1}{2}(\sigma_1-\sigma_3)\frac{\sin 2\theta}{\mu}\right] \tag{6}$$

3.2. Normal-Faulting Stress Regime

Initially (before commencing any fluid injection), major principal stress is vertical stress $\sigma_1=\sigma_{v0}=\int\rho_{sat}gdz$ (where ρ_{sat} is saturated rock density and dz is infinitesimal length in the vertical direction) at a reservoir under the normal-faulting stress regime. Minor principal stress is minimum horizontal stress $\sigma_3=\sigma_{h0}=K\sigma_{v0}$ where $K=\sigma_{h0}/\sigma_{v0}$ denotes initial total horizontal-to-vertical stress ratio. The total stress ratio ranges $0.3+100/z<K<0.5+1500/z$ where z is depth in meter unit [24]. The intermediate principal stress ($\sigma_2=\sigma_{H0}$ in this case; maximum horizontal stress) can be neglected because major and minor principal stresses constitute the largest Mohr circle [25].

Both vertical and horizontal stresses evolve corresponding to pore-pressure buildup Δp and thermally induced stress $\Delta\sigma^T$ during and after the fluid injection:

$$\sigma_v = \sigma_{v0} + \beta_v\Delta p - \Delta\sigma^T \text{ and } \sigma_h = K\sigma_{v0} + \beta_h\Delta p - \Delta\sigma^T \tag{7}$$

By inserting Equation 7 into Equation 6 ($\sigma_1=\sigma_v$, $\sigma_3=\sigma_h$) and rearranging it, we can derive an equation for the maximum pressure limit $p_{max}=p_0+\Delta p_{max}$ as shown below (p_0 represents initial pore pressure):

$$p_{\max} = \frac{1}{\left[2\alpha-\beta_v-\beta_h-(\beta_v-\beta_h)\cos 2\theta+(\beta_v-\beta_h)\sin 2\theta/\mu\right]}\cdot$$

$$\left[\left\{(1+K)+(1-K)\cos 2\theta-(1-K)\sin 2\theta/\mu\right\}\sigma_{v0}\right.$$

$$\left.-\left\{(\beta_v+\beta_h)+(\beta_v-\beta_h)\cos 2\theta-(\beta_v-\beta_h)\sin 2\theta/\mu\right\}p_0-\frac{2\alpha_T E\Delta T}{1-2\nu}\right] \tag{8}$$

3.3. Reverse-Faulting Stress Regime

Maximum horizontal stress is major principal stress $\sigma_{H0}=\sigma_1$ and vertical stress is minor principal stress $\sigma_{v0}=\sigma_3$ at a reservoir under the reverse-faulting stress regime. The horizontal and vertical stresses evolve with respect to pore-pressure buildup and thermal change during and after the fluid injection:

$$\sigma_v = \sigma_{v0} + \beta_v\Delta p - \Delta\sigma^T \text{ and } \sigma_H = K\sigma_{v0} + \beta_h\Delta p - \Delta\sigma^T \tag{9}$$

The initial total stress ratio $K=\sigma_{H0}/\sigma_{v0}$ should be the quotient of maximum horizontal stress to vertical stress in this case. Again, an equation for p_{max} can be derived by inserting Equation 9 into Equation 6 ($\sigma_1=\sigma_H$, $\sigma_3=\sigma_v$) and rearranging it:

$$p_{\max} = \frac{1}{\left[2\alpha-\beta_h-\beta_v-(\beta_h-\beta_v)\cos 2\theta+(\beta_h-\beta_v)\sin 2\theta/\mu\right]}\cdot$$

$$\left[\left\{(K+1)+(K-1)\cos 2\theta-(K-1)\sin 2\theta/\mu\right\}\sigma_{v0}\right.$$

$$\left.-\left\{(\beta_h+\beta_v)+(\beta_h-\beta_v)\cos 2\theta-(\beta_h-\beta_v)\sin 2\theta/\mu\right\}p_0-\frac{2\alpha_T E\Delta T}{1-2\nu}\right] \quad (10)$$

3.4. Strike-Slip Faulting Stress Regime

Maximum horizontal stress is major principal stress $\sigma_{H0}=\sigma_1$ and minimum horizontal stress is minor principal stress $\sigma_{h0}=\sigma_3$ at a reservoir under the strike-slip faulting stress regime (vertical stress is the intermediate principal stress $\sigma_{v0}=\sigma_2$). Here we define a new stress ratio $K_H=\sigma_{h0}/\sigma_{H0}$, which is the initial ratio of total minimum to maximum horizontal stress. These horizontal stresses evolve as pore pressure builds up and temperature drops during and after the cold fluid injection:

$$\sigma_H=\sigma_{H0}+\beta_h\Delta p-\Delta\sigma^T \text{ and } \sigma_h=K_H\sigma_{H0}+\beta_h\Delta p-\Delta\sigma^T \quad (11)$$

An equation for p_{max} can be derived again by inserting Equation 11 into Equation 6 ($\sigma_1=\sigma_H$, $\sigma_3=\sigma_h$):

$$p_{\max}=\frac{1}{\alpha-\beta_h}\left[\left(\frac{1+K_H}{2}+\frac{1-K_H}{2}\cos 2\theta-\frac{1-K_H}{2}\sin 2\theta/\mu\right)\sigma_{H0}-\beta_h p_0-\frac{\alpha_T E\Delta T}{1-2\nu}\right] \quad (12)$$

where θ is the angle between the strike of a fracture plane and minimum horizontal stress.

4. Application

We applied the equations derived in Section 3 to calculating the possible maximum pressure limit for a case study model and compared results with those in the literature. We also conducted sensitivity analysis to examine how parameters influence the maximum sustainable pressure limit.

4.1. A Case Study

We consider a hypothetical axisymmetric model as shown in Figure 1 (the model is originally from Rutqvist et al. [22]). The 1.5-km-deep reservoir is 100 m thick and overlain by 50-m-thick caprock. Mechanical properties are ideal for all layers: Poisson's ratio ν=0.25, Biot's coefficient α=1, Young's modulus E=5GPa, and saturated rock density ρ_{sat}=2260kg/m^3. Initial total vertical stress and pore pressure are σ_{v0}=33.2MPa and p_0=14.7MPa, respectively. Note that permeability and porosity are different for the reservoir and caprock: they affect pore-pressure buildup itself as fluid is injected into a reservoir but do not alter the maximum pressure limit. Zero cohesion c=0 and friction angle of φ=30° (μ=tanφ≈0.6) are assigned for a fracture plane that is assumed to be preferentially existing for imminent shear slip. Two different stress regimes, $\sigma_{h0}=0.7\sigma_{v0}$ (normal-faulting stress regime) and $\sigma_{H0}=1.5\sigma_{v0}$ (reverse-faulting stress regime), were considered in the literature, and numerical simulations were implemented to determine the maximum pressure limit (p_{max}=28MPa and 24MPa, respectively [22]).

First, we examine the normal-faulting stress regime case. We apply the pore-pressure/stress coupling factors β_h=0.61 and β_v=0.31 that are computed at the reservoir-caprock interface for ν=0.25 [26]. Thermal drop was not considered in the literature. Using Equation 8 ($\theta=\pi/4+\varphi/2$ for the critical angle of a fracture plane to shear slip), maximum pressure limit is obtained as p_{max}=28.2MPa. Next, we examine the reverse-faulting stress regime case. We apply the same pore-pressure/stress coupling ratios, and maximum pressure limit is computed as p_{max}=26.1MPa using Equation 10. These similar outcomes (28MPa vs. 28.2MPa and 24MPa vs. 26.1MPa) help us ascertain that the

proposed equations are able to provide reliable maximum-pressure-limit value, given the precise estimate of initial stress state, material properties, and pore-pressure/stress coupling ratios. Even though not included in this application, the set of proposed equations in this study should be able to provide a reliable maximum pressure limit for the nonisothermal cold-fluid injection condition, too, given that a distribution of thermal drop is properly provided, which can be done analytically/numerically using appropriate closed-form solutions.

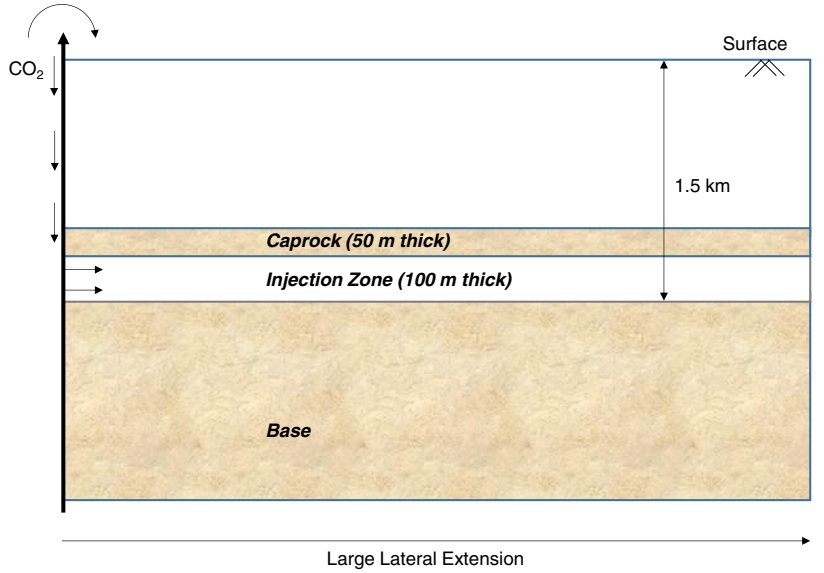

Fig. 1. Hypothetical test model for CO_2 injection and shear slip (ν=0.25 and α=1; original model from Rutqvist et al. [22]).

4.2. Sensitivity Analysis

A benefit of analytical solutions is that we can conduct sensitivity analysis to examine how the maximum pressure limit is sensitive to the probabilistic variation of input parameters. We consider an imaginary 1km-depth reservoir herein and select six parameters that are most likely to affect the maximum pressure limit, based on the derivation in this study. Selected parameters are saturated rock density ρ_{sat}, Biot's coefficient α, Poisson's ratio ν, initial total horizontal-to-vertical stress ratio K, temperature drop at a point of interest ΔT, and Young's modulus E. Lower bound-central value-upper bound for each parameter is 2000kg/m^3-2250kg/m^3-2500kg/m^3 for ρ_{sat}, 0.6-0.8-1 (in case of normal-faulting stress regime) or 1-1.25-1.5 (in case of reverse-faulting stress regime) for K, 0.8-0.9-1 for α, 0.1-0.25-0.4 for ν, 0°C-5°C-10°C for ΔT, and 5GPa-10GPa-15GPa for E. These lower and upper bounds are selected so that they cover most of the possible ranges (except the thermal drop at a point, which could be lower than the range, particularly near the injection well).

Results of the sensitivity analysis, shown in Figure 2, imply that the maximum pressure limit is more sensitive to those reservoir parameters under the normal-faulting stress regime than under the reverse-faulting stress regime (compare the scale of horizontal axis in Fig. 2). The initial total horizontal-to-vertical stress ratio K affects the maximum pressure limit most dominantly for both stress regimes. Therefore, obtaining a precise estimate of the initial stress state that includes vertical, maximum, and minimum horizontal stresses is critical for providing a reliable maximum pressure limit and thus avoiding undesirable induced seismic activities. Poisson's ratio and saturated rock density are the second-most important parameters for determining the maximum pressure limit.

Lastly, note that in this analysis the range of temperature drop was limited to between 0 and 10°C because greater temperature drop could cause a negative pressure limit when directly using equations derived in this manuscript. However, temperature drop in the near field could be greater than 20°C depending on the operation condition (e.g.,

Cranfield pilot test site), so special caution is needed around the injection well for incidents such as hydraulic fractures and drilling-induced failures. Also note that the stress regime itself can transform from one to another (e.g., normal- to reverse-faulting) because of a higher pore-pressure/stress coupling ratio for the horizontal stress $\beta_h > \beta_v$ [26]. If this were to occur, Equations 10 or 12 should be used instead of Equation 8.

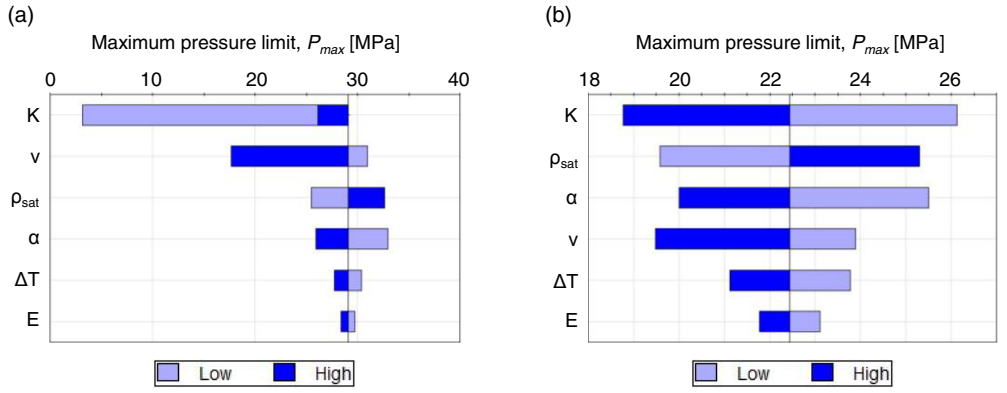

Fig. 2. Tornado plots showing the sensitivity of maximum pressure limit to variation of the probabilistic input parameters at an injection reservoir: (a) normal-faulting stress regime, and (b) reverse-faulting stress regime. Note: fluid density ρ_f=1000kg/m^3, depth to the injection reservoir=1km, porosity=0.25, and coefficient of thermal expansion α_T=1×10^{-5}/K.

5. Conclusions

Mathematical derivation in this study aims at proposing a new set of equations, incorporating pore-pressure/stress coupling and thermal stress effects, with which users can quickly estimate the maximum sustainable pressure limit during the injection of cold pressurized fluid into a geologic formation. Salient observations are as follows:

- A new set of equations for the maximum sustainable pressure limit is proposed, combining the Mohr-Coulomb failure criterion for the reactivation of preexisting fractures with the evolution of total and effective stresses in response to pore-pressure buildup and temperature change. In particular, different equations are derived separately for different stress regimes, including normal-, reverse-, and strike-slip faulting stress regimes.
- Application of the proposed equations into a case study in the literature helps to support the validity of proposed equations. Users can calculate a reliable maximum pressure limit quickly with formulas from this study, given an estimate of initial stress state, material properties, pore-pressure/stress coupling ratios, and thermal diffusion.
- Sensitivity analysis reveals that the maximum pressure limit is more sensitive to input parameters at a reservoir under a normal-faulting stress regime than under a reverse-faulting regime. For both regimes, the initial total horizontal-to-vertical stress ratio influences the maximum pressure limit the most, followed by Poisson's ratio and saturated rock density.

Acknowledgments

This work was funded by the Gulf Coast Carbon Center at the Bureau of Economic Geology (BEG) and the U.S. Department of Energy, NETL, under contract number DE-FE0009301.

References

[1] IEAGHG, Induced Seismicity and its Implication for CO_2 Storage Risk, 2013/09, 2013.
[2] M. Preisig, J.H. Prévost, Coupled multi-phase thermo-poromechanical effects. Case study: CO_2 injection at In Salah, Algeria, International Journal of Greenhouse Gas Control, 5 (2011) 1055-1064.
[3] V. Vilarrasa, S. Olivella, J. Carrera, J. Rutqvist, Long term impacts of cold CO_2 injection on the caprock integrity, International Journal of

Greenhouse Gas Control, 24 (2014) 1-13.
[4] J. Rutqvist, The geomechanics of CO_2 storage in deep sedimentary formations, Geotechnical and Geological Engineering, 30 (2012) 525-551.
[5] J.B. Altmann, T.M. Müller, B.I. Müller, M.R. Tingay, O. Heidbach, Poroelastic contribution to the reservoir stress path, International Journal of Rock Mechanics and Mining Sciences, 47 (2010) 1104-1113.
[6] M. Schoenball, T. Müller, B. Müller, O. Heidbach, Fluid-induced microseismicity in pre-stressed rock masses, Geophysical Journal International, 180 (2010) 813-819.
[7] V. Vilarrasa, J. Carrera, S. Olivella, Hydromechanical characterization of CO_2 injection sites, International Journal of Greenhouse Gas Control, 19 (2013) 665-677.
[8] S. De Simone, V. Vilarrasa, J. Carrera, A. Alcolea, P. Meier, Thermal coupling may control mechanical stability of geothermal reservoirs during cold water injection, Physics and Chemistry of the Earth, Parts A/B/C, 64 (2013) 117-126.
[9] S. Goodarzi, A. Settari, M.D. Zoback, D. Keith, Thermal aspects of geomechanics and induced fracturing in CO_2 injection with application to CO_2 sequestration in Ohio River Valley, in: SPE International Conference on CO_2 Capture Storage and Utilization, Society of Petroleum Engineers, 2010, pp. SPE 139706.
[10] M.A. Addis, The stress-depletion response of reservoirs, in: SPE Annual Technical Conference, 1997, pp. 55-65.
[11] M. Ferronato, G. Gambolati, C. Janna, P. Teatini, Numerical modelling of regional faults in land subsidence prediction above gas/oil reservoirs, International Journal for Numerical and Analytical Methods in Geomechanics, 32 (2008) 633-657.
[12] R.R. Hillis, Pore pressure/stress coupling and its implications for seismicity, Exploration Geophysics-Australia, 31 (2000) 448-454.
[13] R.R. Hillis, Coupled changes in pore pressure and stress in oil fields and sedimentary basins, Petroleum Geoscience, 7 (2001) 419-425.
[14] J.E. Streit, R.R. Hillis, Estimating fault stability and sustainable fluid pressures for underground storage of CO_2 in porous rock, Energy, 29 (2004) 1445-1456.
[15] M.R. Safari, O. Trevor, C. Queena, C. Hamed, N. Blair, M. Uno, C. Hawkes, Effects of depletion/injection induced stress changes on natural fracture reactivation, in: 47th US Rock Mechanics/Geomechanics Symposium, American Rock Mechanics Association, San Francisco, CA, USA, 2013, pp. ARMA 13-395.
[16] J.W. Rudnicki, Fluid mass sources and point forces in linear elastic diffusive solids, Mechanics of Materials, 5 (1986) 383-393.
[17] J. Rutqvist, J. Birkholzer, C.F. Tsang, Coupled reservoir–geomechanical analysis of the potential for tensile and shear failure associated with CO_2 injection in multilayered reservoir–caprock systems, International Journal of Rock Mechanics and Mining Sciences, 45 (2008) 132-143.
[18] V. Vilarrasa, O. Silva, J. Carrera, S. Olivella, Liquid CO_2 injection for geological storage in deep saline aquifers, International Journal of Greenhouse Gas Control, 14 (2013) 84-96.
[19] C. Doughty, B. Freifeld, Modeling CO_2 injection at Cranfield, Mississippi: Investigation of methane and temperature effects, Greenhouse Gases: Science and Technology, 3 (2013) 475-490.
[20] S. Kim, S.A. Hosseini, Above-zone pressure monitoring and geomechanical analyses for a field-scale CO_2 injection project in Cranfield, MS, Greenhouse Gases: Science and Technology, 4 (2013).
[21] Z. Luo, Modeling injection induced fractures and their impact in CO_2 geological storage, in: Petroleum and Geosystems Engineering, University of Texas at Austin, Ph.D., Austin, 2013.
[22] J. Rutqvist, J. Birkholzer, F. Cappa, C.F. Tsang, Estimating maximum sustainable injection pressure during geological sequestration of CO_2 using coupled fluid flow and geomechanical fault-slip analysis, Energy Conversion and Management, 48 (2007) 1798-1807.
[23] S. Vidal-Gilbert, E. Tenthorey, D. Dewhurst, J. Ennis-King, P. Van Ruth, R. Hillis, Geomechanical analysis of the Naylor Field, Otway Basin, Australia: Implications for CO_2 injection and storage, International Journal of Greenhouse Gas Control, 4 (2010) 827-839.
[24] E. Brown, E. Hoek, Trends in relationships between measured *in-situ* stresses and depth, in: International Journal of Rock Mechanics and Mining Sciences & Geomechanics Abstracts, Elsevier, Pergamon, 1978, pp. 211-215.
[25] C.D. Hawkes, P. McLellan, S. Bachu, Geomechanical factors affecting geological storage of CO_2 in depleted oil and gas reservoirs, Journal of Canadian Petroleum Technology, 44 (2005).
[26] S. Kim, S.A. Hosseini, Pore pressure/stress coupling during fluid injection and its implications for CO_2 geological storage, Under review, (2014).